



HAL
open science

Talin and kindlin cooperate to control the density of integrin clusters

Julien Pernier, Marcelina Cardoso Dos Santos, Mariem Souissi, Adrien Joly, Hemalatha Narassimprakash, Olivier Rossier, Grégory Giannone, Emmanuèle Helfer, Kheya Sengupta, Christophe Le Clainche

► **To cite this version:**

Julien Pernier, Marcelina Cardoso Dos Santos, Mariem Souissi, Adrien Joly, Hemalatha Narassimprakash, et al.. Talin and kindlin cooperate to control the density of integrin clusters. *Journal of Cell Science*, 2023, 136, pp.jcs260746. 10.1242/jcs.260746 . hal-03873344

HAL Id: hal-03873344

<https://hal.science/hal-03873344v1>

Submitted on 24 Nov 2023

HAL is a multi-disciplinary open access archive for the deposit and dissemination of scientific research documents, whether they are published or not. The documents may come from teaching and research institutions in France or abroad, or from public or private research centers.

L'archive ouverte pluridisciplinaire **HAL**, est destinée au dépôt et à la diffusion de documents scientifiques de niveau recherche, publiés ou non, émanant des établissements d'enseignement et de recherche français ou étrangers, des laboratoires publics ou privés.

RESEARCH ARTICLE

Talin and kindlin cooperate to control the density of integrin clusters

Julien Pernier^{1,*}, Marcelina Cardoso Dos Santos^{1,*}, Mariem Souissi², Adrien Joly³, Hemalatha Narassimprakash¹, Olivier Rossier³, Grégory Giannone³, Emmanuèle Helfer², Kheya Sengupta² and Christophe Le Clainche^{1,‡}

ABSTRACT

Focal adhesions are composed of transmembrane integrins, linking the extracellular matrix to the actomyosin cytoskeleton, via cytoplasmic proteins. Adhesion depends on the activation of integrins. Talin and kindlin proteins are intracellular activators of integrins that bind to β -integrin cytoplasmic tails. Integrin activation and clustering through extracellular ligands guide the organization of adhesion complexes. However, the roles of talin and kindlin in this process are poorly understood. To determine the contribution of talin, kindlin, lipids and actomyosin in integrin clustering, we used a biomimetic *in vitro* system, made of giant unilamellar vesicles, containing transmembrane integrins (herein α IIb β 3), with purified talin (talin-1), kindlin (kindlin-2, also known as FERMT2) and actomyosin. Here, we show that talin and kindlin individually have the ability to cluster integrins. Talin and kindlin synergize to induce the formation of larger integrin clusters containing the three proteins. Comparison of protein density reveals that kindlin increases talin and integrin density, whereas talin does not affect kindlin and integrin density. Finally, kindlin increases integrin–talin–actomyosin coupling. Our study unambiguously demonstrates how kindlin and talin cooperate to induce integrin clustering, which is a major parameter for cell adhesion.

KEY WORDS: Actin, Integrin, Kindlin, Membrane, Talin

INTRODUCTION

Cell adhesion and migration are controlled by biochemical and mechanical signals from the environment. These stimuli trigger the remodeling of the cytoskeleton and modify its attachment to the extracellular matrix (ECM), via focal adhesions (FAs). FAs are major mechanosensitive complexes made of integrin transmembrane receptors that mechanically couple the ECM to the actomyosin cytoskeleton, via actin-binding proteins (ABPs) such as talin proteins (talin-1 and talin-2 in mammals; hereafter talin is used generically, except when referring to the *in vitro* experimental

system). Integrins are heterodimers composed of an α -subunit and a β -subunit linked by non-covalent interactions. There are 24 combinations of different heterodimers (Kechagia et al., 2019) that share an organization made of two extracellular parts that associate to bind ligands, two transmembrane helices and two cytoplasmic tails interacting with a variety of adaptors and regulators. The platelet α IIb β 3 integrin, used as a model integrin in this study, plays a critical role in hemostasis and thrombosis (Coller and Shattil, 2008; Li et al., 2010).

In cells, early adhesion processes involve the formation of integrin nanoclusters and the recruitment of numerous ABPs that polymerize actin at the leading edge. In response to actomyosin contraction, these actin-linked nanoclusters grow to form stable FAs that elongate and increase the strength of their adhesion to the ECM (Yu et al., 2011). This process depends on both the activation of individual integrins and their clustering, and that of the associated components, to increase the adhesion surface and the avidity for ligands. Clustering requires integrin diffusion and is promoted by the association of integrins to extracellular ligands and intracellular regulators.


A nanolithographic study has revealed that the organization of extracellular integrin ligands into nanoclusters, in which the ligands bind precisely spaced integrins, is a critical parameter for cell adhesion, in contrast to the average density of these extracellular ligands (Schvartzman et al., 2011). However, Coyer et al., using nanopatterning of fibronectin, conclude that this spacing limit is not a constant. Indeed, its value depends on multiple parameters, such as the adhesive force, cytoskeletal tension and the force-transmitting intracellular adaptor proteins (Coyer et al., 2012).

Integrins are also controlled by intracellular regulators that modulate both their affinity for extracellular ligands and adhesion area by promoting their clustering. Talin is a major regulator of integrin (Das et al., 2014). Talin is a large multidomain protein, composed of a N-terminal head domain, containing a FERM (4.1, ezrin, radixin moesin) domain (F1 to F3), followed by a flexible linker and a large rod domain, made of 13 consecutive α -helical bundles (R1 to R13), and a C-terminal dimerization domain (Ciobanasu et al., 2013; Goult et al., 2018). Talin also contains three actin-binding sites (ABS) (Hemmings et al., 1996) located in the F2 and F3 subdomains of the head, the R4 to R8 bundles and the C-terminal part including the R13 bundle and the C-terminal dimerization helix. The F3 subdomain of the FERM domain binds to the membrane proximal NPxY motif in the cytoplasmic tail of β integrin subunit to induce an ‘inside-out’ allosteric conformational change, allowing integrins to bind ECM with high affinity (Bachmann et al., 2019; Wehrle-Haller, 2012). This mechanism requires the highly positively charged subdomains of talin head to bind with membrane phosphatidylinositol 4,5-bisphosphate (PIP₂). The binding of the talin head to the inner membrane leaflet

¹Université Paris-Saclay, CEA, CNRS, Institute for Integrative Biology of the Cell (I2BC), 91198, Gif-sur-Yvette, France. ²Aix Marseille Univ, CNRS, CINAM, Turing Centre for Living Systems, Marseille, France. ³Université de Bordeaux, CNRS, Interdisciplinary Institute for Neuroscience, IINS, UMR 5297, F-33000 Bordeaux, France.

*These authors contributed equally to this work

‡Author for correspondence (christophe.leclainche@i2bc.paris-saclay.fr)

 J.P., 0000-0002-0480-9355; M.C.D.S., 0000-0003-2004-1777; H.N., 0000-0002-9995-5071; O.R., 0000-0002-6932-931X; G.G., 0000-0002-0932-1690; E.H., 0000-0001-8123-0964; K.S., 0000-0002-1060-2713; C.L.C., 0000-0001-5659-677X

containing PIP₂ allows a lysine residue to be brought closer to a membrane proximal site in the β -integrin subunit to disrupt an electrostatic interaction between the α and β cytoplasmic tails, resulting in an active conformation that is prone to clustering (Saltel et al., 2009; Wegener et al., 2007). Mechanical unfolding of talin helical bundles by mechanical forces produced by actin polymerization and actomyosin contraction exposes binding sites for the ABP vinculin, which promotes talin-dependent integrin activation and clustering, and reinforces the anchoring of integrins to the actin cytoskeleton (Atherton et al., 2015; Ciobanasi et al., 2014; del Rio et al., 2009; Hirata et al., 2014; Yang et al., 2014). It is debated whether talin dimerization is important for integrin clustering. On the one hand, overexpression of talin lacking the dimerization domain impairs FA formation (Atherton et al., 2015). On the other hand, the expression of talin without this domain in talin-knockout cells rescues the formation of normal FAs (Austen et al., 2015). Integrin clustering mediated by talin could also be enhanced by the self-assembly of PIP₂ into membrane clusters in the presence of divalent cations (Wen et al., 2018). Thus, the mechanisms of integrin clustering are still poorly understood.

Along with talin, kindlin proteins are major regulators of integrins (Larjava et al., 2008). The kindlin family (kindlin-1, -2 and -3, also known as FERMT1, FERMT2 and FERMT3, respectively; hereafter kindlin is used generically, except when referring to the *in vitro* experimental system) comprises three isoforms that share the same conserved domain architecture. Like talin, kindlin contains a FERM domain (F1 to F3), that binds to a membrane distal NxxY motif in the cytoplasmic tail of the β -integrin subunit, which is distinct from the proximal one that binds the talin FERM domain. This FERM domain is required for integrin activation and clustering (Bouaouina et al., 2012; Goult et al., 2009; Moser et al., 2009). The FERM domain of kindlin is interrupted by an additional pleckstrin homology (PH) domain inserted in F2 that recognizes membrane phosphoinositides, with higher affinity for phosphatidylinositol (3,4,5)-trisphosphate (PIP₃) than for PIP₂ (Li et al., 2017; Liu et al., 2011). This domain triggers the localization of kindlin at the membrane and promotes its diffusion, allowing kindlin to reach and activate integrins (Orré et al., 2021).

Although studies in cells, based on overexpression or deletion of several isoforms of talin and kindlin, have established that these two regulators cooperate in integrin activation (Anthis et al., 2009; Calderwood et al., 1999; Ma et al., 2008; Montanez et al., 2008; Moser et al., 2009; Tadokoro et al., 2003), the molecular mechanism underlying this synergy is unclear. The binding of talin and kindlin to different sites along the cytoplasmic tail of β -integrin subunit is likely involved in this mechanism. Recent molecular dynamics simulations have suggested that the binding of kindlin to the distal site of the cytoplasmic tail of β -integrin subunit enhances the interaction of talin with the membrane proximal site, leading to the dissociation of α and β integrin cytoplasmic tails (Haydari et al., 2020). However, measurement of integrin activation, using purified integrins inserted into membrane nanodiscs, indicates that kindlin alone is not capable of activating integrins. Moreover, it also rules out a role for kindlin in talin-dependent activation of single integrins (Ye et al., 2013). Instead, the same study showed that, in cells, kindlin increases integrin affinity for multivalent but not monovalent extracellular ligands, suggesting a role for kindlin in talin-activated integrin clustering. Interestingly, tracking of single proteins in cells has revealed that talin associates with integrins in FAs from a cytoplasmic pool (Rossier et al., 2012), whereas kindlin membrane diffusion allows it to reach FAs and activate integrins (Orré et al., 2021). Furthermore, the association of kindlin with

integrins is more labile than that of talin, indicating that these two regulators might also act sequentially or independently of each other.

PIP₂ and PIP₃ have been found to have a critical role for the function of proteins that act as adaptors between the membrane and the actin cytoskeleton at sites of adhesion (Di Paolo and De Camilli, 2006). Thus, we first investigated the impact of PIP₂ on integrin clustering and adaptor recruitment. Furthermore, although the role of extracellular ligands in driving integrin clustering is well known, the role of intracellular molecular assemblies is not yet clear. In this work, we tested our hypothesis that intracellular components, such as talin and kindlin can independently trigger integrin clustering. We also determined the contribution of kindlin in integrin–talin–actomyosin coupling.

To determine the contribution of integrin, talin, kindlin, lipids and actomyosin in integrin clustering, we performed experiments with a minimal *in vitro* reconstituted system, made of giant unilamellar vesicles (GUVs) containing or not inactive transmembrane α IIb β 3 integrins, on which purified talin-1, kindlin-2, actin and myosin II assemble. We first compare the effect of different phosphoinositides on talin and kindlin recruitment. Our results indicate that the fraction of membrane-bound talin and kindlin depends on the density of PIP₂ and PIP₃, with talin having a higher affinity for PIP₂, while kindlin has a higher affinity for PIP₃. Then, using GUVs containing integrins with and without PIP₂, we determine the effect of integrin activation by Mn²⁺ and the influence of talin and kindlin on integrin clustering. While inactive integrin alone is homogeneously distributed in the membrane, Mn²⁺ triggers the formation of integrin clusters, demonstrating that integrin activation leads to its clustering. Addition of talin or kindlin, in the presence of PIP₂, induces their co-clustering with integrin. For talin, this effect does not depend on its dimerization. When added together, talin and kindlin synergize to induce the formation of larger integrin clusters than those observed in the presence of each protein alone. Quantification of protein density in talin–kindlin–integrin clusters reveals that kindlin increases the density of both talin and integrin, while talin does not alter the density of kindlin and integrin. Finally, in the presence of talin, kindlin increases integrin segregation in membrane tubes stretched from GUVs by actomyosin contraction, suggesting that kindlin enhances integrin–talin–actomyosin coupling. Our study reveals how kindlin and talin synergize to induce integrin clustering, thereby enhancing cell adhesion.

RESULTS

Phosphoinositides control talin and kindlin recruitment at the surface of GUVs

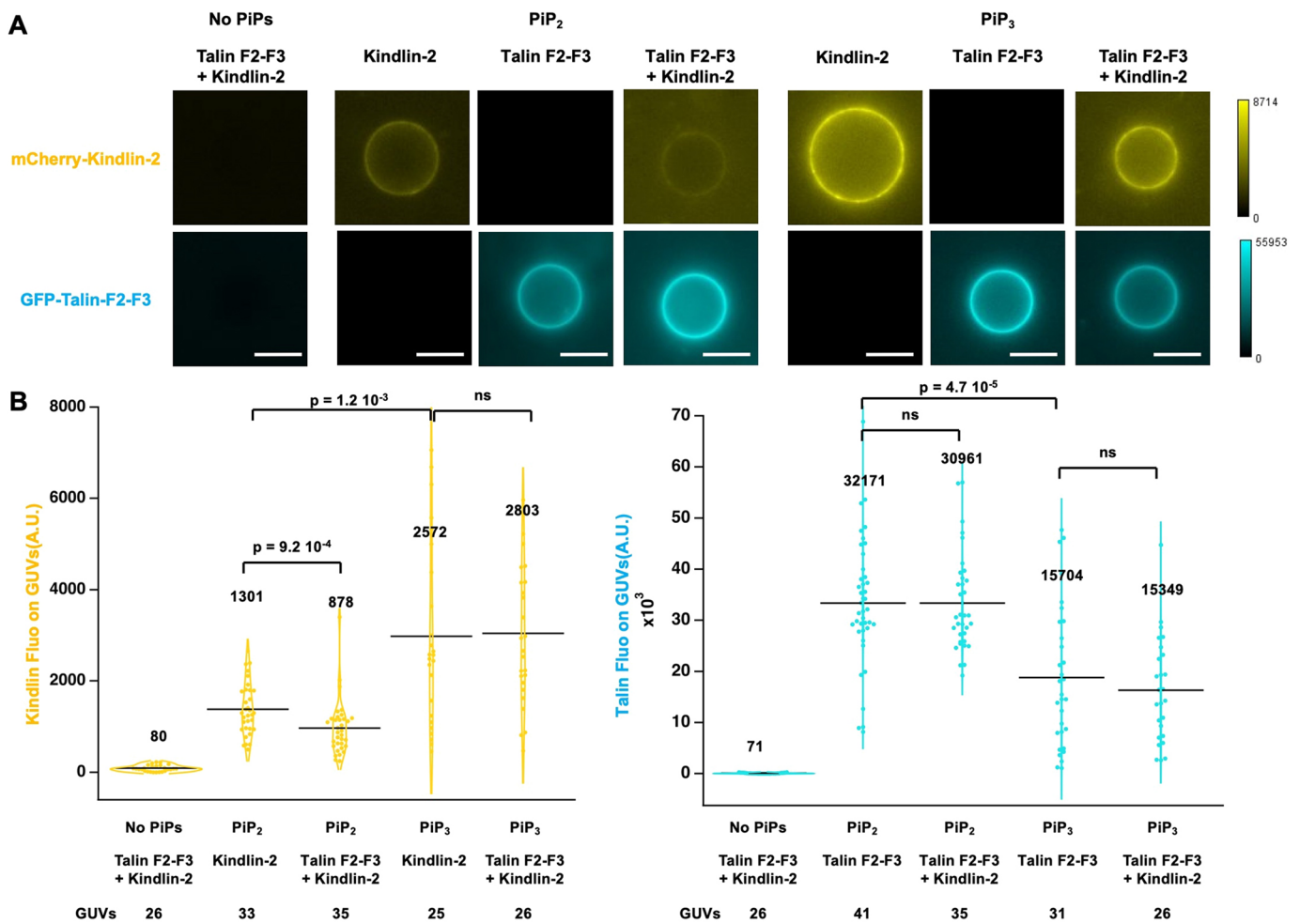
Localization of talin and kindlin at the plasma membrane is crucial for integrin activation and FA formation (Chinthalapudi et al., 2018; Orré et al., 2021). Before studying the clustering of integrins by its activators talin and kindlin, we first determined whether these proteins associate to the membrane of giant unilamellar vesicles (GUVs) without integrins. We measured the recruitment of these proteins by fluorescence microscopy at the surface of GUVs. We used a fluorescent eGFP-fused construct of talin-1, encompassing the F2 and F3 subdomains that contains most of the PIP₂-binding interface, and mCherry-fused full-length kindlin-2. Given that several studies have proposed that talin and kindlin have different specificities for phosphoinositides, we compared their binding to GUVs containing PIP₂ (5% mole) or PIP₃ (5% mole). We choose a lipid composition allowing efficient incorporation of integrins into preteoliposomes (Souissi et al., 2021) with concentrations similar to

those found in cell membrane (Ikonen, 2008; Martin, 2012). The lipid mixtures we used contain L- α -phosphatidylcholine (egg PC) with 20% mole cholesterol alone, or supplemented with 5% mole PIP₂ or 5% mole PIP₃. Although this composition reflects the average content of the membrane, it should be noted that the synthesis of PIP₃ is dynamically regulated, and it is quickly dephosphorylated.

As a control, we first showed that neither talin nor kindlin bind to GUVs that do not contain phosphoinositides (Fig. 1A). Kindlin binds to GUVs containing PIP₂ but the fluorescence signal is on average 2-fold higher for GUVs containing PIP₃, indicating a higher affinity for this phosphoinositide (Fig. 1A,B). By contrast, talin has a higher affinity for PIP₂ than for PIP₃, as shown by the 2-fold higher fluorescence signal on the violin plot (Fig. 1B). The surface density of phosphoinositides is not a limiting parameter in our assays because both talin and kindlin are recruited when they are added together. Under all conditions, talin and kindlin distributions were homogeneous on the GUV surface and no clusters were detected. In conclusion, phosphoinositides are not self-assembling in the presence of integrin activators and are not sufficient to initiate clustering.

Talin and kindlin recruitment induces integrin clustering

To determine whether and how talin and kindlin influence integrin clustering, we used GUVs containing transmembrane α IIb β 3 integrins, with or without PIP₂ and the previously used fluorescent talin F2F3 domain and full-length kindlin-2. The α IIb β 3 integrin is expressed in megakaryocytes where kindlin-3 is expressed, rather than kindlin-2 (Bialkowska et al., 2015; Moser et al., 2008). Although kindlin-2 and kindlin-3 are homologous in sequence and share 67% similarity, their regulation and functional roles in adhesion are rather different (Kadry et al., 2020). However, the integrin β 3 subunit, together with other α -subunits, is expressed in many cell types expressing kindlin-2. As kindlin interacts with the β -subunit of integrin, our model system has sufficient relevance. The talin F2-F3 construct contains a binding site in F3 for the membrane proximal NPxY motif of the cytoplasmic tail of β -integrin. This F3-NPXY interaction has been shown to be sufficient to activate α IIb β 3 integrin in cells (Tadokoro et al., 2003). Inactive α IIb β 3 integrins, from human platelets, were purified and labelled with Alexa Fluor 647 as previously described (Souissi et al., 2021). Integrins were first inserted into proteoliposomes after removal of detergent from Triton-lipid micelles (Rigaud and Lévy,



2003; Souissi et al., 2021; Streicher et al., 2009). GUVs containing integrins were then prepared by the electroformation technique (Fig. S1) (Angelova et al., 1992). Inactive integrins, in the absence

of ligands or activators, were homogeneously distributed in the membrane of GUVs (Fig. 2A). Importantly, addition of Mn^{2+} , which is known to activate integrins (Hynes, 2002; Takagi et al.,

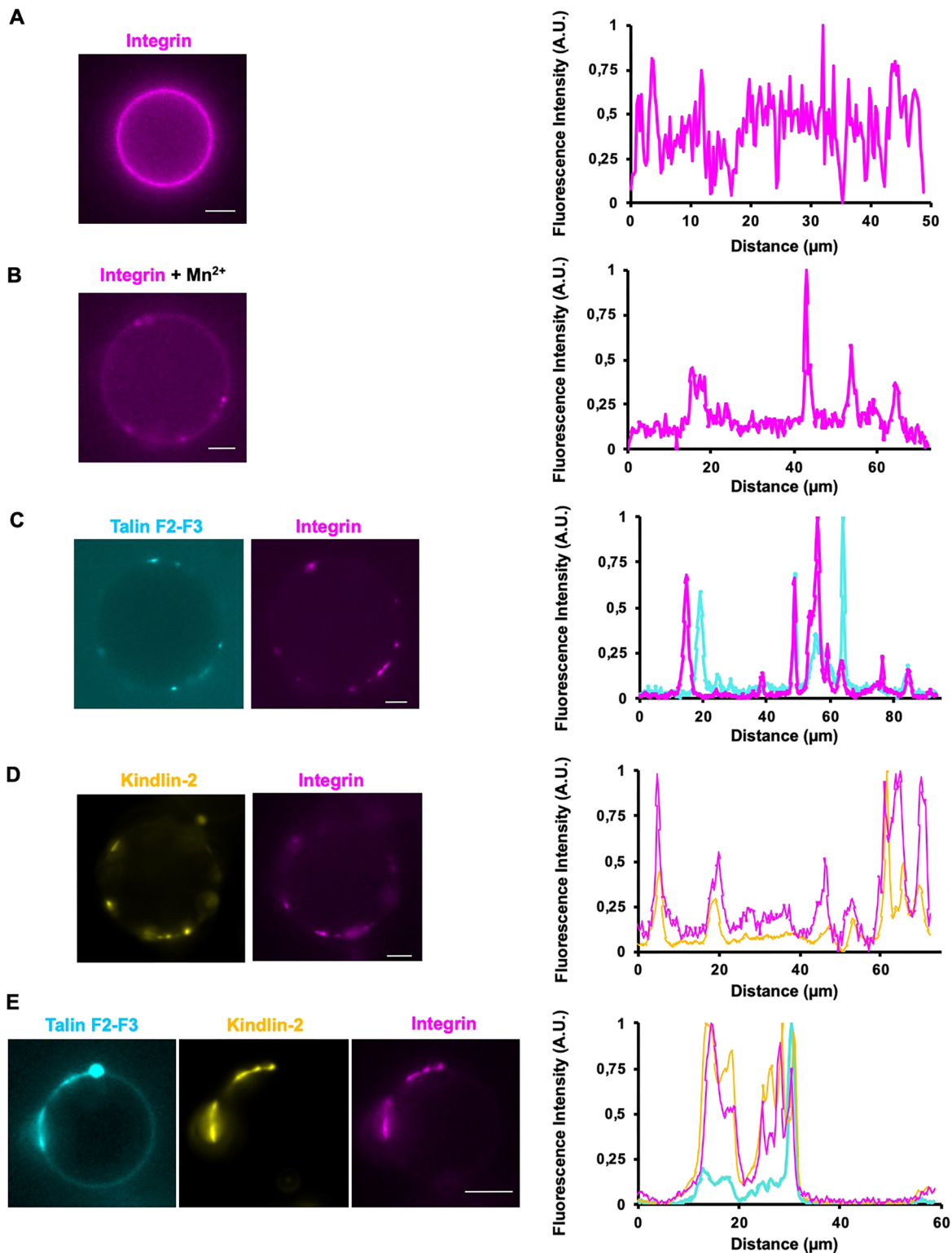


Fig. 2. Talin and kindlin recruitment on integrin-containing GUVs induces formation of clusters. (A–E) Representative epifluorescence images (left) of Alexa Fluor 647-labeled integrin (magenta) reconstituted into GUVs incubated without (A) or with $MnCl_2$ (B, 2 mM) alone, eGFP–talin F2-F3 (cyan, C, 200 nM) alone, mCherry–kindlin-2 (yellow, D, 200 nM) alone, or eGFP–talin F2-F3 (200 nM) and mCherry–kindlin-2 (200 nM) in combination (E). Corresponding plot profiles (right) of the normalized fluorescence signals of the different proteins on the contours of the corresponding GUVs are shown. The observations presented in this figure were confirmed in 2 to 4 independent experiments depending on the conditions. Scale bars: 5 μm . A.U., arbitrary units.

2002), triggered the formation of integrin clusters (Fig. 2B; Fig. S3) in the absence or presence of PIP₂, demonstrating that activation is involved in clustering. This experiment also demonstrated that our purified integrins inserted in GUVs are activable. Without PIP₂, no recruitment of talin F2F3 and kindlin-2 was observed at the surface of integrin-containing GUVs (Fig. S3). Interestingly, in GUVs containing both integrin and PIP₂, talin F2F3 colocalized with integrins in clusters of a few micrometers in length, which is close to the size of focal adhesions (Fig. 2C). A similar integrin density was measured using a longer talin construct (F2-F3-R1-R2-R3-R13) including the C-terminal dimerization domain (Figs S1, S4). We concluded that talin dimerization is not required for integrin clustering. All these results suggest a clustering mechanism that involves lateral intermolecular interactions between different integrins activated by talin binding. Surprisingly, the addition of kindlin-2 alone also leads to the formation of integrin clusters (Fig. 2D). This was not expected because kindlin alone does not induce the active conformation of integrins (Ye et al., 2013). This result implies that kindlin acts by different mechanisms. A first possibility is that the mechanism involves kindlin dimerization or its higher order oligomerization. An alternative would be that kindlin induces a conformational change of integrin that has not yet been reported and which is prone to clustering. The combined addition of talin and kindlin promotes the formation of much larger clusters where integrin, talin and kindlin colocalize (Fig. 2E). These results demonstrate a hierarchical clustering of integrins involving integrin activation and binding to intracellular activators. Owing to the brownian movement of GUVs and the diffusion of clusters in the

plane of the membrane, we could not follow the real-time formation of clusters.

Talin and kindlin regulate the length and density of integrin clusters

To understand the hierarchy of the clustering activities of the proteins that comprise our assay and to estimate their organization within the clusters, we quantified the effect of each protein alone or in combination on the length of the clusters and the density of each protein. The length was calculated using the ‘Spot detector’ plugin (Icy software). The density of proteins in clusters was analyzed using a previously established method based on fluorescence measurements (Prévost et al., 2017; Sorre et al., 2012; see Materials and Methods section and Fig. S2). The integrin clusters induced by the addition of Mn²⁺, talin alone or kindlin alone had a similar length (Fig. 3A). Moreover, cluster length was comparable based on values obtained from the talin channel (Fig. 3B) and the kindlin channel (Fig. 3C). This latter observation rules out a mechanism in which an initial core of talin- or kindlin-bound integrins would attract free integrins into clusters, but rather indicates that each integrin must be associated with talin or kindlin to join a cluster.

Interestingly, the protein density in integrin–kindlin co-clusters is higher than in the integrin–talin co-clusters described above, confirming that kindlin and talin act on integrin organization through different mechanisms (Fig. 3D). By combining talin, kindlin and integrin-containing GUVs, we observed the emergence of larger clusters characterized by a high density of integrin and talin (Fig. 3D,E) that were comparable to those observed with kindlin

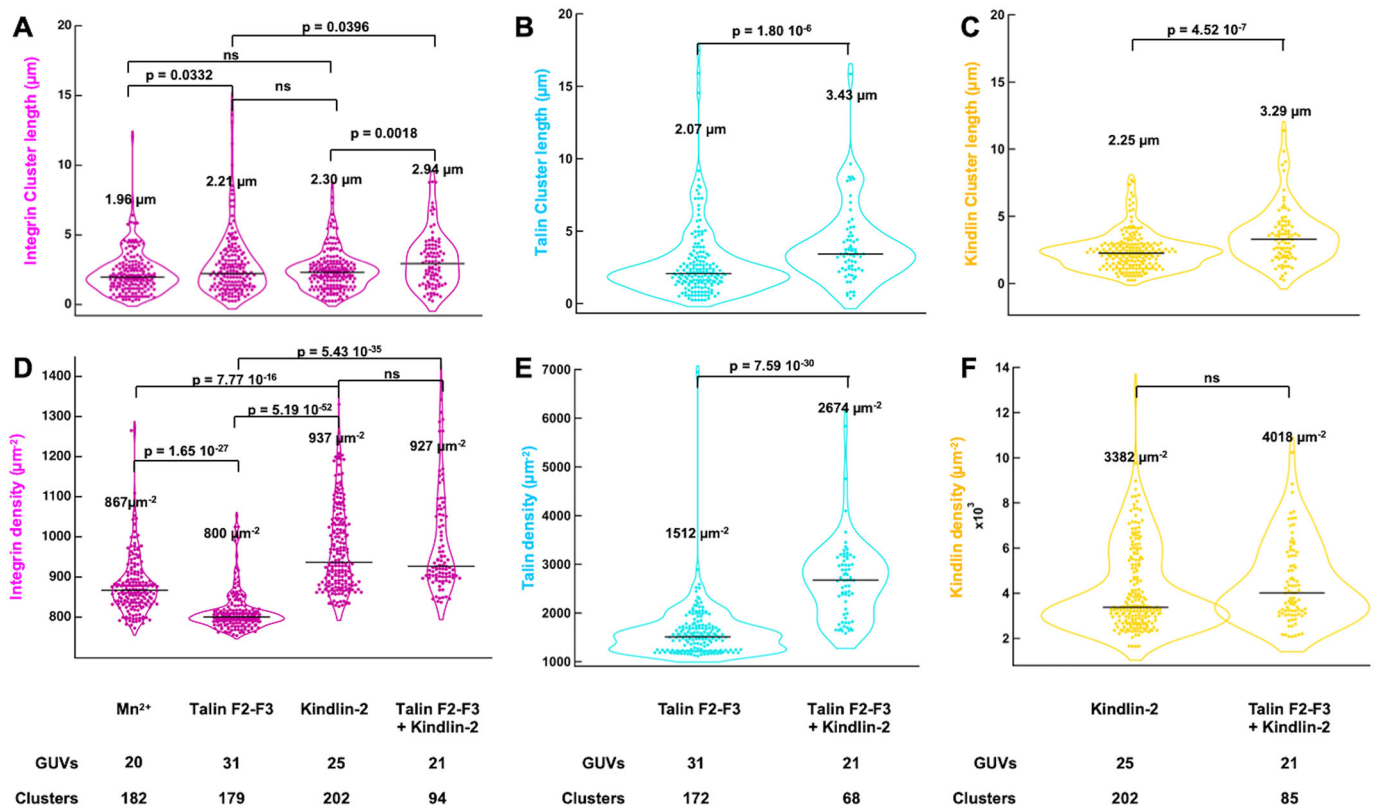


Fig. 3. Talin and kindlin regulate integrin clusters length and density. Violin representation of the length (A–C) and the density (D–F) of integrin (magenta), talin (cyan) and kindlin (yellow) clusters in the presence of MnCl₂ (2 mM) alone, eGFP–talin F2-F3 (200 nM) alone, mCherry–kindlin-2 (200 nM) alone, or eGFP–talin F2-F3 (200 nM) and mCherry–kindlin-2 (200 nM) in combination. The number of analyzed GUVs, clusters and the medians (black lines) are indicated. The results presented in this figure were confirmed in 2 to 4 independent experiments depending on the conditions. The *P*-values were obtained by a Mann–Whitney non-parametric test at level 0.05. ns, not significant.

alone (Fig. 3D,F). These results clearly indicate that the density of the three proteins is controlled by kindlin. The fact that the distributions of integrin densities were very spread out and that the measured values overlapped for the talin alone, kindlin alone and talin with kindlin conditions indicates that there is a continuum of integrin densities and that kindlin simply increases integrin density in talin-induced clusters.

Analysis of the density distributions of the different proteins in the clusters also provides us with an estimate of their average stoichiometry within the different clusters. As clusters diffuse and GUVs rotate, our sequential acquisition setup did not allow us to calculate the stoichiometry of each protein pair in the individual clusters but only the ratios of the means of the protein density distributions. Thus, after a fluorescence calibration of each component, we were able to establish that the average stoichiometry of talin–integrin co-clusters is 2:1, whereas the average stoichiometry of kindlin–integrin co-clusters is 3:1 and clusters containing talin, kindlin and integrin show an average stoichiometry of 3:4:1 (Fig. 3). Similar distributions of GUVs perimeters were observed in the different conditions (Fig. S5A). No correlation was observed between the distributions of perimeters of GUVs and the different properties of the clusters such as their length or density (Fig. S5B,C).

Kindlin increases integrin–talin–actomyosin coupling

To explore the influence of kindlin on the association between talin–integrin and a contractile actomyosin cytoskeleton, we repeated the previous experiments with a construct of talin (F2-F3-R1-R2-R3-R13) comprising the F2-F3 subdomains of the head, followed by the first three helical bundles (R1-R2-R3) and finishing by the R13 helical bundle and the dimerization domain corresponding to an actin binding site (ABS3). This talin construct binds to PIP₂-containing GUVs through F2 and F3, to integrin through F3 and

transmits force by anchoring to actomyosin through its ABS3 domain (Vigouroux et al., 2020). As mentioned above, this construct has the same efficiency in forming integrin clusters as talin F2F3 (Fig. S4).

We first observed the effect of adding polymerizing actin filaments in the presence of myosin II, which generates, through its contractile activity, a pulling force on integrin via talin. The spectacular effect that we noticed immediately is the massive deformation of GUVs by actomyosin that results in the stretching of tubes and formation of small vesicles containing integrin (Fig. 4C₄) and coated with actin (Fig. 4A₄), whereas no such structures are observed in the presence of actin alone (Fig. 4A₃,C₃). This effect would not be readily observed in cells because integrins are usually anchored to extracellular ligands that resist membrane deformation. In the presence of talin alone, a proportion of the integrins colocalized with actomyosin, where the formation of tubes indicates force application (Fig. 4A₄,C₄). Addition of kindlin together with talin seemed to increase the fraction of integrins in regions of GUVs that are mechanically deformed by actomyosin (Fig. 4A₅,C₅). Strikingly, all kindlin density was found colocalized with actomyosin (Fig. 4B₅). This observation is not related to the direct interaction between kindlin-2 and actin filaments proposed by a recent study (Bledzka et al., 2016), because in the presence of kindlin alone we did not observe the recruitment of actomyosin on GUVs (Fig. 4A₂). However, it is possible that the interaction of kindlin with the membrane and integrin prevents its binding to actin. In this series of experiments, the recruitment of proteins into the tubes emerging from the GUVs corresponds to low intensities compared to the background, and a portion of these structures is not always in the plane of focus of the microscope, resulting in heterogeneous fluorescence intensities between conditions A₄–C₄ and A₅–C₅. We therefore preferred to quantify the surface extension of integrin-containing tubes relative to the original GUV surface,

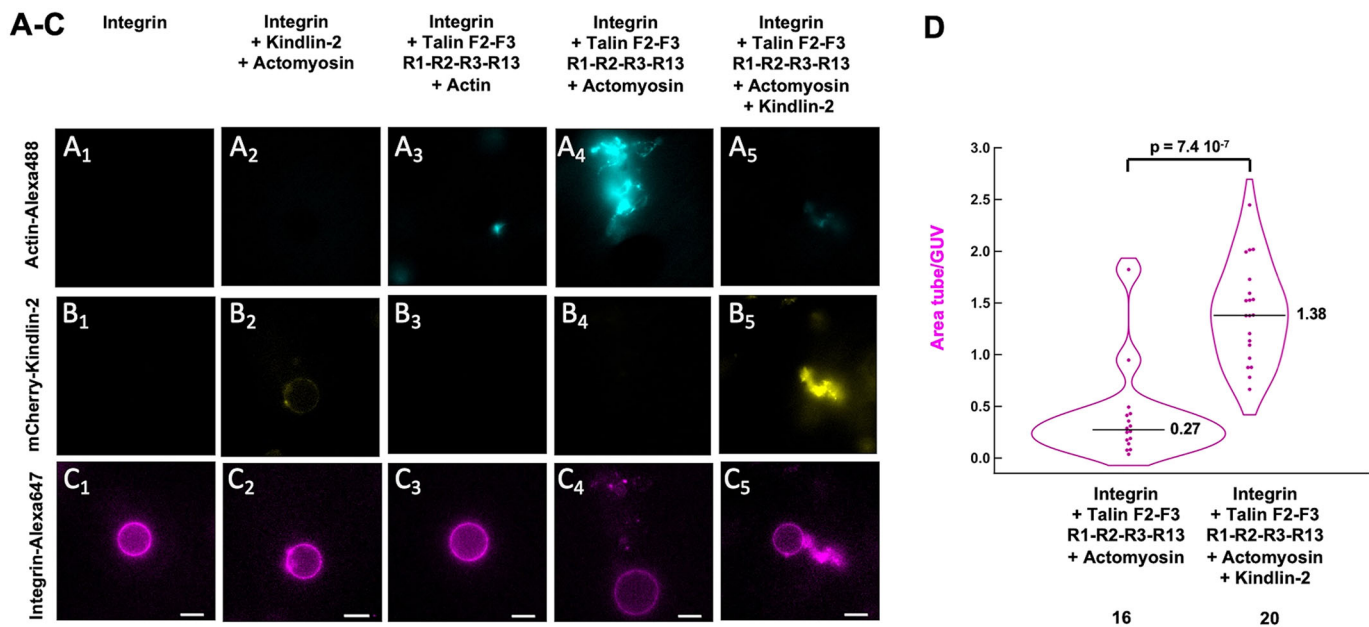


Fig. 4. Kindlin enhances the actomyosin-dependent segregation of integrins. (A–C) Representative epifluorescence images of integrin (magenta) containing GUVs without and with actin (2 μM, 2% Alexa Fluor 488 labeled, cyan) and myosin II (50 nM), supplemented with talin F2-F3-R1-R2-R3-R13 (200 nM), mCherry-kindlin-2 (200 nM, yellow), and both talin and kindlin. The mean background was subtracted for each image. Scale bars: 10 μm. (D) Violin representation of tubes area (μm²) normalized by GUV area (μm²) quantified from the integrin–Alexa Fluor 647 channel. The number of analyzed GUVs and the medians are indicated. The results presented in this figure were confirmed in 2 to 4 independent experiments depending on the conditions. The *P*-values were obtained by a Mann–Whitney non-parametric test at level 0.05. ns, not significant.

which is independent of integrin fluorescence intensity. As the tubes become longer, the surface area of the GUV decreases. The ratio between the areas of integrin-containing tubes and GUVs increased significantly in the presence of talin and kindlin (Fig. 4D, right), compared to what was seen for the talin-only condition (Fig. 4D, left). Collectively these observations indicate that kindlin increases integrin–talin–actomyosin coupling.

DISCUSSION

How talin and kindlin control the activation and clustering of integrins to initiate the formation of FAs in cells remains largely unclear. In this work, the roles of integrin activation, talin and kindlin in integrin clustering were investigated using an *in vitro* biomimetic system. We demonstrate here that the F2 and F3 subdomains of talin and kindlin-2 organize integrins into clusters independently, and synergistically when added together, through the binding to their respective sites along the β -integrin cytoplasmic tail. In this process, kindlin controls the density of talin and integrins (Fig. 5).

Although the mechanism that leads to the formation of talin, kindlin and integrin co-clusters is not completely understood, using

our results, we can rule out some possibilities and propose some hypotheses. First, we have experimentally eliminated the possibility that talin and PIP₂ without integrin form clusters. Second, the fact that a monomeric talin (F2F3) induces integrin cluster formation excludes a molecular mechanism based on the formation of a regular 2D network of talin–integrins on the membrane surface. Indeed, talin would have to be dimeric for this to occur. Also, in our *in vitro* system, integrin clustering does not require the interaction mediated by the F1 talin loop with the integrin tail, as previously described (Kukkurainen et al., 2020). We propose that the talin-activated integrin acquires the ability to self-assemble, which fits with the clustering we observed upon Mn²⁺ activation of integrin. Interestingly, a series of studies in cells and on model membranes has suggested that clustering of activated integrins is related to the homomeric or heteromeric oligomerization of integrins transmembrane helices (Berger et al., 2010; Li et al., 2003; Li et al., 2005; Ye et al., 2014). The mechanism involved in kindlin clustering seems to differ from that of talin. First, protein density is higher in kindlin-induced clusters. Second, it has been shown that kindlin oligomerization is required in FA formation (Bu et al., 2021; Li et al., 2017; Ye et al., 2013). Therefore, kindlin might

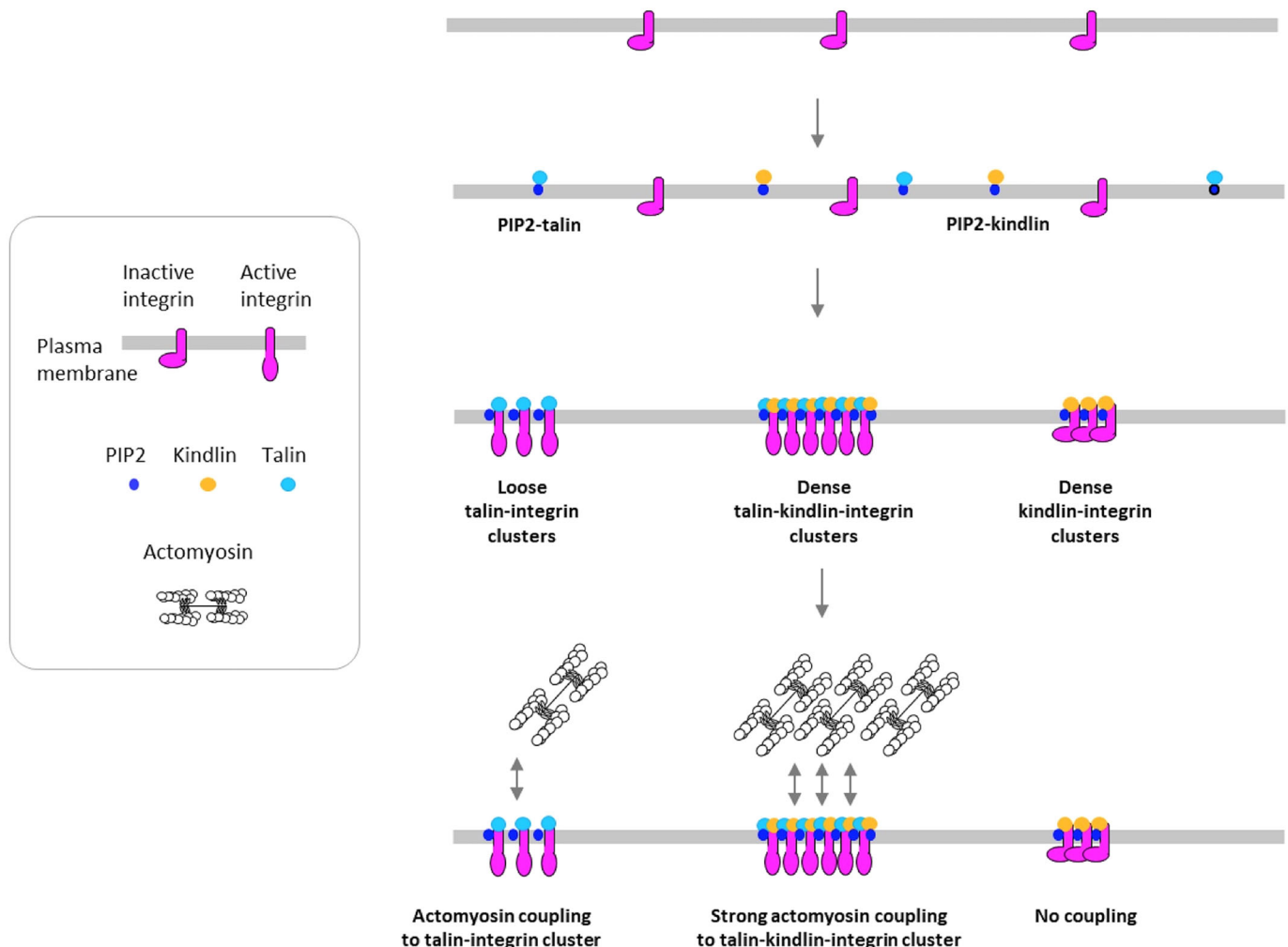


Fig. 5. Working model showing how talin and kindlin cooperate to control the density of integrin clusters and their coupling to actomyosin. Talin and kindlin are recruited to membrane via PIP2 and PIP3, specifically (only PIP2 is represented), allowing for their interaction with diffusive integrins in the membrane. Binding to talin activates integrins, which become able to self-assemble into clusters that can recruit actomyosin. In contrast, kindlin induces clustering of inactive integrins into denser clusters that are unable to bind actomyosin. When combined, kindlin dictates the high density of talin and integrin in clusters and enhances their coupling to actomyosin. See Discussion for further details.

act as an adaptor to enhance integrin clusters. Various models with different types of cooperation have been suggested to explain the synergy between talin and kindlin (Lu et al., 2022; Moser et al., 2009; Sun et al., 2019). Here, we have shown that it is kindlin that dictates the density of talin and integrin in clusters. Our results provide details of the mechanism underlying the role of kindlin in the previously observed clustering of integrins in cells (Ye et al., 2013).

The existence of two isoforms of talin, three isoforms of kindlin and 24 integrin heterodimers suggests that there could be differences in integrin cluster characteristics depending on their composition in isoforms, such as cluster size and protein density. In particular, it would be interesting to compare the ability of kindlin-2 and kindlin-3 to cluster β 1- and β 3-containing integrins that exhibit different dynamic behavior within FAs (Rossier et al., 2012). The broad protein density distributions measured in our experiments also suggest that talin–kindlin–integrin complexes with different stoichiometries coexist in the clusters. As our experimental strategy only allows the calculation of average stoichiometries, it will be interesting to determine these values by single-molecule measurements. Our study has also demonstrated that local phosphoinositide distribution might affect the balance between talin and kindlin within clusters. The ability of cells to produce adhesive plaques containing varying densities of integrin might play a role in the recognition of different densities of extracellular ligands.

The role of actin polymerization and actomyosin force in all stages of adhesion complex formation has been the subject of numerous studies in cells. Actin polymerization might act as an assembly platform that facilitates integrin clustering via mechanisms that remain largely to be understood but may involve ABPs such as talin, vinculin, the Arp2/3 complex and others (Ciobanasi et al., 2013; Yu et al., 2011). Our results show that actin is not required for the formation of large integrin clusters. In cells, actomyosin contraction allows fusion of nascent clusters and their retrograde movement backwards where they anchor the cell body (Yu et al., 2011). In our *in vitro* system, where GUVs are free to move in all directions, it is difficult to capture cluster fusion and movement in real time. However, the fact that actomyosin drives segregation of integrins under mechanical force, as revealed by membrane deformation, supports such a scenario.

The development of our experimental system has allowed us to understand some of the elementary reactions that govern the self-assembly and organization of adhesion complexes. The absence of extracellular ligands allowed us to isolate the intracellular reactions that accompany inside-out integrin activation. However, the contribution of outside-in integrin signaling plays a role, and it will be important to determine how the spatial organization and mechanical properties of extracellular ligands influence the organization of clusters induced intracellularly by talin and kindlin, and vice versa. It might be possible to develop planar systems with supported lipid bilayers containing integrins and add ligands, or to develop synthetic cells with integrin regulators encapsulated within them (Kelley et al., 2020; Litschel et al., 2021).

MATERIALS AND METHODS

Key resources are listed in Table S1.

Protein expression purification and labeling

The enhanced green fluorescent protein (eGFP)-tagged talin F2-F3 was cloned into a pGEX-6P1 plasmid, with a cleavable N-terminal glutathione-S-transferase (GST) tag followed by eGFP. The talin F2-F3-R1-R2-R3-R13 cDNA was cloned into a pETM plasmid with a N-terminal StrepTagII and a C-terminal 6His tag. The mCherry-kindlin 2 cDNA was cloned into a

pGEX-6P1 plasmid, with a cleavable N-terminal Glutathione-S-transferase (GST) tag followed by mCherry and with a C-terminal 6His tag.

All recombinant proteins were expressed in *Escherichia coli* BL21 DE3 (Invitrogen), in LB medium, with induction by 1 mM IPTG at 16°C overnight.

EGFP-talin F2-F3 was bound to glutathione–Sephacryl, cleaved by PreScission protease and purified by gel filtration chromatography (Superdex 200, 16/60, GE Healthcare) in 20 mM Tris-HCl pH 8.5, 150 mM KCl, 1 mM β -mercaptoethanol (BME), frozen in liquid nitrogen, and stored at -80°C .

Talin F2-F3-R1-R2-R3-R13 was bound to Ni-NTA-Agarose resin and eluted with 250 mM imidazole and dialyzed in 20 mM Tris-HCl pH 7.8, 100 mM KCl and 1 mM DTT, frozen in liquid nitrogen and stored at -80°C .

mCherry-kindlin 2 was bound on a HisTrap FF crude column (GE Healthcare) and eluted with 300 mM imidazole. Pooled protein fractions were bound to GSTrap column cleaved by PreScission protease and purified by gel filtration chromatography (Superdex 200, 16/60) in 20 mM Tris-HCl pH 7.8, 100 mM NaCl, 1 mM BME, concentrated using Vivaspinn (10 kDa), frozen in liquid nitrogen, and stored at -80°C .

Integrin α IIb β 3 was purified as previously described (Souissi et al., 2021). Briefly, integrin was extracted from outdated human platelets from French Blood Establishment (EFS) with 1% Triton X-100 and purified via affinity chromatography over Concanavalin A, heparin–Sephacryl, and KYGRGDS columns (HiPrep 16/60 Sephacryl S-300 HR). The functionality of the integrins was verified by checking the ability to bind on the KYGRGDS column upon addition and removal of 2 mM MnCl_2 . Proteins were isolated in pure inactivated form by size exclusion chromatography (Sephacryl S300 16/60). Purified integrins were labeled with Alexa Fluor 647 succinimidyl ester following the manufacturer's protocol (Thermo Fisher Scientific). Integrins were frozen in liquid nitrogen and stored at -80°C in a buffer containing detergent (20 mM HEPES pH 7.5, 150 mM NaCl, 1 mM CaCl_2 , 1 mM MgCl_2 , 0.1% Triton X-100 and 0.01% NaN_3).

Actin was purified from rabbit muscle and isolated in monomeric form in G buffer (5 mM Tris-HCl pH 7.8, 0.1 mM CaCl_2 , 0.2 mM ATP, 1 mM DTT and 0.01% NaN_3). Actin was labeled with Alexa Fluor 488 succinimidyl ester-NHS (Ciobanasi et al., 2015).

Myosin II was purified from rabbit muscle following the method described by Pollard (Pollard, 1982). The rabbit muscle samples used for the actin and myosin purifications were taken in the Experimental Unit (UE 1298) INRAE Ile-de-France - Jouy-en-Josas - Antony and are subject to a declaration to the DDPP (Direction Départementale de la Protection des Populations) des Yvelines.

Integrin reconstitution in proteoliposomes

Integrin was reconstituted in proteoliposomes by detergent-mediated method (Rigaud and Lévy, 2003). A lipid mixture of 75% mole EPC, 20% mole cholesterol and 5% mole PIP_2 , in chloroform at a concentration of 1 mg/ml was vacuum-dried overnight. Dry lipidic film was resuspended at 6 mg/ml in integrin buffer (20 mM HEPES pH 7.5, 150 mM NaCl, 1 mM CaCl_2 , 1 mM MgCl_2 , and 0.01% NaN_3) at detergent:lipid ratios of 2.5 (w/w) for Triton X-100 by incubation at room temperature (RT) for 30 min under agitation. Then, integrin α IIb β 3 was added at a protein:lipid ratio of 1:5000 to obtain a final lipid concentration of 3 mg/ml. After 15 min incubation at RT, the detergent was removed by two successive additions of an amount of Bio-beads equivalent to a beads-to-detergent ratio of 10 (w/w), then a third one with a ratio of 20 (w/w), with respective incubation at RT for 2 h, 1 h and 1 h under agitation. The obtained solution was stored at -20°C for up to 4 weeks.

GUV preparation

GUVs were prepared by using a modified version of the polyvinyl alcohol (PVA) gel-assisted vesicle formation method (Weinberger et al., 2013). Briefly, PVA was dissolved at 5% (w/w) in a 280 mM sucrose solution containing 20 mM Tris-HCl pH 7.5. The PVA solution, heated to 50°C , was spread onto 22×22 mm glass coverslips, previously cleaned by sonication in Milli-Q water (Merck), ethanol and Milli-Q water sequentially (10 min

each). The PVA-coated coverslips were incubated at 40°C for 3 h. Lipids were mixed in chloroform at a concentration of 1 mg/ml. The lipid mixtures we used contain L- α -phosphatidylcholine (egg PC) with 20% mole cholesterol alone, or supplemented with 5% mole brain L- α -phosphatidylinositol-4,5-bisphosphate (PIP₂) or 5% mole 1,2-dioleoyl-sn-glycero-3-phospho-(1'-myo-inositol-3',4',5'-trisphosphate) (PIP₃). 10 μ l of each lipid mixture was spread on the PVA-coated coverslips using a Hamilton syringe and partially vacuum-dried for 30 min at RT. Around 1 ml of 200 mM sucrose solution was added on the top of the coverslips. GUVs were formed by incubation at least 2 h at RT. Finally, the GUVs were collected, centrifuged at 14,000 g for 30 min, and stored in glass vials at 4°C for up to 1 week.

GUVs containing integrins were prepared by the electroformation technique (Angelova et al., 1992). 10 droplets of 1 μ l of the proteoliposome solution (3 mg/ml) were deposited onto both indium tin oxide (ITO)-coated glass slides. The film was then partially vacuum-dried for 30 min. After partial dehydration, a home-made electroformation chamber was built and was filled with ~6 ml 200 mM sucrose solution. For electroformation, the content was exposed to an AC electric field, incremented from 0.2 V up to 0.8 V every 30 min (0.2 V steps), at 10 Hz frequency, and left overnight. Then, the AC frequency was lowered to 4 Hz for 30 min with an AC electric field of 0.2 V to detach the giant vesicles from the glass slide. Finally, the GUVs were collected, centrifuged at 14,000 g for 30 min, and stored in glass vials at 4°C for up to 1 week.

GUV assays

For all experiments, coverslips were passivated with PLL-g-PEG. Coverslips were sequentially cleaned by sonication with milli-Q water, ethanol and milliQ water for 10 min, then irradiated for 1 min under a deep UV lamp, incubated for 1 h in 0.1 mg/ml PLL-g-PEG dissolved in 10 mM HEPES pH 7.8 and washed with milliQ H₂O. Finally, an observation chamber was created by attaching the passivated coverslip to a Petri dish lacking a bottom. To maintain the stability of the GUVs, the experiments were performed in an observation buffer containing 50 mM KCl and 110 mM glucose. GUVs were added to a solution containing the different proteins. The GUV-protein mixture was incubated for at least 20 min before observation to allow protein recruitment and sedimentation of GUVs. The final concentration of proteins, if present, were: 200 nM eGFP-talin F2-F3, 200 nM mCherry-kindlin 2, 200 nM talin F2-F3-R1-R2-R3-R13, 50 nM myosin II and 2 μ M actin with 2% Alexa Fluor 488 labeled. A stock of actin (2% Alexa Fluor 488 labeled) at 40 μ M was prepared in G Buffer containing 0.2 mM ATP and diluted 20 times to 2 μ M. In the GUV assay, 20 μ l of this stock was added in a final volume of 400 μ l. The final concentration of ATP was 10 μ M, which allows actin polymerization.

Samples were observed by epifluorescence with an Olympus IX71 microscope equipped with a 60 \times oil immersion objective and coupled to a Cascade II EMCCD (Photometrics) camera.

Quantification of mCherry-kindlin 2 and eGFP-talin F2-F3 at the surface of GUVs

The data were quantified by measuring the averaged fluorescence signal along the equatorial section of the vesicles, with background subtraction. The violin representations were assembled with Igor Pro.

Characterization of the length and density of protein clusters

We measured the protein surface density (number of proteins per unit area) on GUVs by using a previously established method (Prévost et al., 2017; Sorre et al., 2012). It is calculated from a labeled proteins/lipids calibration. We first measured the fluorescence of EPC GUVs containing predefined amounts of fluorescent lipids – Atto647-DOPE, Fluorescein-DOPE and Sulforhodamine-DHPE (respectively, DOPE*₆₄₇, DOPE*_F and DHPE*_R) to establish the relationship between the density (respectively, $n_{DOPE^*_{647}}$, $n_{DOPE^*_{F}}$ and $n_{DHPE^*_{R}}$) and the corresponding fluorescence intensity (respectively, $I_{DOPE^*_{647}}^{GUV}$, $I_{DOPE^*_{F}}^{GUV}$ and $I_{DHPE^*_{R}}^{GUV}$) (Fig. S2). Assuming an area per egg PC of 0.68 nm², we derive the respective calibration coefficients A_1 , A_2 and A_3 , corresponding to the slopes of the following curves (1, 2 and 3). Note that A_1 , A_2 and A_3 depend on the illumination and recording settings of

the microscope.

$$n_{DOPE^*_{647}} = A_1 \times I_{DOPE^*_{647}}^{GUV} \quad (1)$$

$$n_{DOPE^*_{F}} = A_2 \times I_{DOPE^*_{F}}^{GUV} \quad (2)$$

$$n_{DHPE^*_{R}} = A_3 \times I_{DHPE^*_{R}}^{GUV} \quad (3)$$

Given that integrin is labeled with Alexa Fluor 647 and not Atto647, we have to correct A_1 by the ratio of fluorescence of the two fluorescent dyes in bulk deduced from the slope of the titration curves (Fig. S2). We then obtained the surface density of integrin deduced from the measurement of the integrin-Alexa Fluor 647 intensity $I_{Integrin}$ as:

$$n_{Integrin} = \frac{A_1}{\frac{I_{Alexa647}}{I_{DOPE^*_{647}}} \times Z_1} \times I_{Integrin} \quad (4)$$

As talin is labeled with eGFP and not fluorescein, we have to correct A_2 by the ratio of fluorescence of the two fluorescent dyes in bulk deduced from the slope of the titration curves (Fig. S2). We then obtained the surface density of talin deduced from the measurement of the eGFP-talin intensity I_{Talin} as:

$$n_{Talin} = \frac{A_2}{\frac{I_{GFP}}{I_{DOPE^*_{F}}} \times Z_2} \times I_{Talin} \quad (5)$$

As kindlin is labeled with mCherry and not rhodamine, we have to correct A_3 by the ratio of fluorescence of the two fluorescent dyes in bulk deduced from the slope of the titration curves (Fig. S2). We then obtained the surface density of kindlin deduced from the measurement of the mCherry-kindlin intensity $I_{Kindlin}$ as:

$$n_{Kindlin} = \frac{A_3}{\frac{I_{mCherry}}{I_{DHPE^*_{R}}} \times Z_3} \times I_{Kindlin}, \quad (6)$$

where Z represents the degree of labeling for the protein of interest: $Z_1=1.73$, $Z_2=1$, $Z_3=1$. In our experiments, the calibration factors are the following:

$\frac{A_1}{\frac{I_{Alexa647}}{I_{DOPE^*_{647}}} \times Z_1}$ is equal to 0.298, $\frac{A_2}{\frac{I_{GFP}}{I_{DOPE^*_{F}}} \times Z_2}$ is equal to 0.204 and

$\frac{A_3}{\frac{I_{mCherry}}{I_{DHPE^*_{R}}} \times Z_3}$ is equal to 0.208.

Measurements of clusters length and density and GUVs perimeters were performed using the Spot Detector plugin, with Size Filtering Method, bright detection and scale 3 and sensitivity of 75, in Icy software (Institut Pasteur, France Bio Imaging; Boquet-Pujadas et al., 2021). The length of the clusters corresponds to the maximum Ferret diameter which is the maximum distance between any two points of the surface.

Quantification of Alexa Fluor 647-integrin segregation

The contours of the areas containing the stretched integrin tubes and the GUV were defined as corresponding to a threshold integrin fluorescence intensity corresponding to values 10% higher than the background value, using the raw images without background correction. These measurements of tubes and GUVs area were performed using ImageJ software.

Statistical analysis

The graphs were assembled using Igor Pro or Kaleidagraph. Statistical analysis was performed using a Mann-Whitney non-parametric test in Microsoft Excel.

Acknowledgements

We thank P. Bassereau (Institut Curie, Paris, France) and R. Jaffiol (UTT, Troyes) for insightful discussions.

Competing interests

The authors declare no competing or financial interests.

Author contributions

Conceptualization: C.L.C.; Methodology: J.P., M.C.D.S., M.S., A.J., H.N.; Formal analysis: J.P., M.C.D.S., C.L.C.; Investigation: J.P., M.C.D.S.; Writing - original draft: J.P., C.L.C.; Writing - review & editing: J.P., M.C.D.S., O.R., G.G., E.H., K.S., C.L.C.; Visualization: M.C.D.S.; Supervision: C.L.C.; Project administration: C.L.C.; Funding acquisition: G.G., K.S., C.L.C.

Funding

This research was funded by grants from Agence Nationale de la Recherche (ANR-18-CE13-0026-01 to C.L.C., G.G. and K.S., ANR-20-CE13-0016 to C.L.C. and ANR-21-CE13-0010-03 to C.L.C.).

Data availability

All relevant data can be found within the article and its supplementary information.

References

- Angelova, M. I., Soléau, S., Méléard, Ph., Faucon, F. and Bothorel, P. (1992). Preparation of giant vesicles by external AC electric fields. Kinetics and applications. In *Trends in Colloid and Interface Science VI*, Vol. 89 (ed. C. Helm, M. Lösche, and H. Mähwald), pp. 127-131. Steinkopff. doi:10.1007/BFb0116295
- Anthis, N. J., Wegener, K. L., Ye, F., Kim, C., Goult, B. T., Lowe, E. D., Vakonakis, I., Bate, N., Critchley, D. R., Ginsberg, M. H. et al. (2009). The structure of an integrin/talin complex reveals the basis of inside-out signal transduction. *EMBO J.* **28**, 3623-3632. doi:10.1038/emboj.2009.287
- Atherton, P., Stutchbury, B., Wang, D.-Y., Jethwa, D., Tsang, R., Meiler-Rodriguez, E., Wang, P., Bate, N., Zent, R., Barsukov, I. L. et al. (2015). Vinculin controls talin engagement with the actomyosin machinery. *Nat. Commun.* **6**, 10038. doi:10.1038/ncomms10038
- Austen, K., Ringer, P., Mehlich, A., Chrostek-Grashoff, A., Kluger, C., Klingner, C., Sabass, B., Zent, R., Rief, M. and Grashoff, C. (2015). Extracellular rigidity sensing by talin isoform-specific mechanical linkages. *Nat. Cell Biol.* **17**, 1597-1606. doi:10.1038/ncb3268
- Bachmann, M., Kukkurainen, S., Hytönen, V. P. and Wehrle-Haller, B. (2019). Cell adhesion by integrins. *Physiol. Rev.* **99**, 1655-1699. doi:10.1152/physrev.00036.2018
- Berger, B. W., Kulp, D. W., Span, L. M., Degrado, J. L., Billings, P. C., Senes, A., Bennett, J. S. and Degrado, W. F. (2010). Consensus motif for integrin transmembrane helix association. *Proc. Natl. Acad. Sci. USA* **107**, 703-708. doi:10.1073/pnas.0910873107
- Bialkowska, K., Byzova, T. V. and Plow, E. F. (2015). Site-specific phosphorylation of kindlin-3 protein regulates its capacity to control cellular responses mediated by integrin α IIb β 3. *J. Biol. Chem.* **290**, 6226-6242. doi:10.1074/jbc.M114.634436
- Bledzka, K., Bialkowska, K., Sossey-Alaoui, K., Vaynberg, J., Pluskota, E., Qin, J. and Plow, E. F. (2016). Kindlin-2 directly binds actin and regulates integrin outside-in signaling. *J. Cell Biol.* **213**, 97-108. doi:10.1083/jcb.201501006
- Boquet-Pujadas, A., Olivo-Marin, J.-C. and Guillén, N. (2021). Bioimage analysis and cell motility. *Patterns* **2**, 100170. doi:10.1016/j.patter.2020.100170
- Bouaouina, M., Goult, B. T., Huet-Calderwood, C., Bate, N., Brahme, N. N., Barsukov, I. L., Critchley, D. R. and Calderwood, D. A. (2012). A conserved lipid-binding loop in the Kindlin FERM F1 domain is required for kindlin-mediated α IIb β 3 integrin coactivation. *J. Biol. Chem.* **287**, 6979-6990. doi:10.1074/jbc.M111.330845
- Bu, W., Levitskaya, Z., Tan, S.-M. and Gao, Y.-G. (2021). Emerging evidence for kindlin oligomerization and its role in regulating kindlin function. *J. Cell Sci.* **134**, jcs256115. doi:10.1242/jcs.256115
- Calderwood, D. A., Zent, R., Grant, R., Rees, D. J. G., Hynes, R. O. and Ginsberg, M. H. (1999). The Talin head domain binds to integrin β subunit cytoplasmic tails and regulates integrin activation. *J. Biol. Chem.* **274**, 28071-28074. doi:10.1074/jbc.274.40.28071
- Chinthalapudi, K., Rangarajan, E. S. and Izard, T. (2018). The interaction of Talin with the cell membrane is essential for integrin activation and focal adhesion formation. *Proc. Natl. Acad. Sci. USA* **115**, 10339-10344. doi:10.1073/pnas.1806275115
- Ciobanasu, C., Faivre, B. and Le Clairche, C. (2013). Integrating actin dynamics, mechanotransduction and integrin activation: The multiple functions of actin binding proteins in focal adhesions. *Eur. J. Cell Biol.* **92**, 339-348. doi:10.1016/j.ejcb.2013.10.009
- Ciobanasu, C., Faivre, B. and Le Clairche, C. (2014). Actomyosin-dependent formation of the mechanosensitive talin-vinculin complex reinforces actin anchoring. *Nat. Commun.* **5**, 3095. doi:10.1038/ncomms4095
- Ciobanasu, C., Faivre, B. and Le Clairche, C. (2015). Reconstituting actomyosin-dependent mechanosensitive protein complexes in vitro. *Nat. Protoc.* **10**, 75-89. doi:10.1038/nprot.2014.200
- Coller, B. S. and Shattil, S. J. (2008). The GPIIb/IIIa (integrin α IIb β 3) odyssey: A technology-driven saga of a receptor with twists, turns, and even a bend. *Blood* **112**, 3011-3025. doi:10.1182/blood-2008-06-077891
- Coyer, S. R., Singh, A., Dumbauld, D. W., Calderwood, D. A., Craig, S. W., Delamarque, E. and Garcia, A. J. (2012). Nanopatterning reveals an ECM area threshold for focal adhesion assembly and force transmission that is regulated by integrin activation and cytoskeleton tension. *J. Cell Sci.* **125**, 5110-5123. doi:10.1242/jcs.108035
- Das, M., Subbayya Ithychanda, S., Qin, J. and Plow, E. F. (2014). Mechanisms of talin-dependent integrin signaling and crosstalk. *Biochim. Biophys. Acta Biomembr.* **1838**, 579-588. doi:10.1016/j.bbmem.2013.07.017
- Del Rio, A., Perez-Jimenez, R., Liu, R., Roca-Cusachs, P., Fernandez, J. M. and Sheetz, M. P. (2009). Stretching single talin rod molecules activates vinculin binding. *Science* **323**, 638-641. doi:10.1126/science.1162912
- Di Paolo, G. and De Camilli, P. (2006). Phosphoinositides in cell regulation and membrane dynamics. *Nature* **443**, 651-657. doi:10.1038/nature05185
- Goult, B. T., Bouaouina, M., Harburger, D. S., Bate, N., Patel, B., Anthis, N. J., Campbell, I. D., Calderwood, D. A., Barsukov, I. L., Roberts, G. C. et al. (2009). The structure of the N-terminus of kindlin-1: a domain important for α IIb β 3 integrin activation. *J. Mol. Biol.* **394**, 944-956. doi:10.1016/j.jmb.2009.09.061
- Goult, B. T., Yan, J. and Schwartz, M. A. (2018). Talin as a mechanosensitive signaling hub. *J. Cell Biol.* **217**, 3776-3784. doi:10.1083/jcb.201808061
- Haydari, Z., Shams, H., Jahed, Z. and Mofrad, M. R. K. (2020). Kindlin Assists Talin to Promote Integrin Activation. *Biophys. J.* **118**, 1977-1991. doi:10.1016/j.bpj.2020.02.023
- Hemmings, L., Rees, D. J., Ohanian, V., Bolton, S. J., Gilmore, A. P., Patel, B., Priddle, H., Trevithick, J. E., Hynes, R. O. and Critchley, D. R. (1996). Talin contains three actin-binding sites each of which is adjacent to a vinculin-binding site. *J. Cell Sci.* **109**, 2715-2726. doi:10.1242/jcs.109.11.2715
- Hirata, H., Tatsumi, H., Lim, C. T. and Sokabe, M. (2014). Force-dependent Vinculin binding to Talin in live cells: A crucial step in anchoring the actin cytoskeleton to focal adhesions. *Am. J. Physiol. Cell Physiol.* **306**, C607-C620. doi:10.1152/ajpcell.00122.2013
- Hynes, R. O. (2002). Integrins. *Cell* **110**, 673-687. doi:10.1016/S0092-8674(02)00971-6
- Ikonen, E. (2008). Cellular cholesterol trafficking and compartmentalization. *Nat. Rev. Mol. Cell Biol.* **9**, 125-138. doi:10.1038/nrm2336
- Kadry, Y. A., Maisuria, E. M., Huet-Calderwood, C. and Calderwood, D. A. (2020). Differences in self-association between kindlin-2 and kindlin-3 are associated with differential integrin binding. *J. Biol. Chem.* **295**, 11161-11173. doi:10.1074/jbc.RA120.013618
- Kechagia, J. Z., Ivaska, J. and Roca-Cusachs, P. (2019). Integrins as biomechanical sensors of the microenvironment. *Nat. Rev. Mol. Cell Biol.* **20**, 457-473. doi:10.1038/s41580-019-0134-2
- Kelley, C. F., Litschel, T., Schumacher, S., Dedden, D., Schwille, P. and Mizuno, N. (2020). Phosphoinositides regulate force-independent interactions between talin, vinculin, and actin. *Elife* **9**, e56110. doi:10.7554/eLife.56110
- Kukkurainen, S., Azizi, L., Zhang, P., Jacquier, M.-C., Baikoghli, M., Von Essen, M., Tuukkanen, A., Laitaoja, M., Liu, X., Rahikainen, R. et al. (2020). The F1 loop of the talin head domain acts as a gatekeeper in integrin activation and clustering. *J. Cell Sci.* **133**, jcs239202. doi:10.1242/jcs.239202
- Larjava, H., Plow, E. F. and Wu, C. (2008). Kindlins: essential regulators of integrin signalling and cell-matrix adhesion. *EMBO Rep.* **9**, 1203-1208. doi:10.1038/embor.2008.202
- Li, R., Mitra, N., Gratkowski, H., Vilaire, G., Litvinov, R., Nagasami, C., Weisel, J. W., Lear, J. D., Degrado, W. F. and Bennett, J. S. (2003). Activation of integrin α IIb β 3 by modulation of Transmembrane Helix Associations. *Science* **300**, 795-798. doi:10.1126/science.1079441
- Li, W., Metcalf, D. G., Gorelik, R., Li, R., Mitra, N., Nanda, V., Law, P. B., Lear, J. D., Degrado, W. F. and Bennett, J. S. (2005). A push-pull mechanism for regulating integrin function. *Proc. Natl. Acad. Sci. USA* **102**, 1424-1429. doi:10.1073/pnas.0409334102
- Li, Z., Delaney, M. K., O'Brien, K. A. and Du, X. (2010). Signaling during platelet adhesion and activation. *Arterioscler. Thromb. Vasc. Biol.* **30**, 2341-2349. doi:10.1161/ATVBAHA.110.207522
- Li, H., Deng, Y., Sun, K., Yang, H., Liu, J., Wang, M., Zhang, Z., Lin, J., Wu, C., Wei, Z. et al. (2017). Structural basis of kindlin-mediated integrin recognition and activation. *Proc. Natl. Acad. Sci. USA* **114**, 9349-9354. doi:10.1073/pnas.1703064114
- Litschel, T., Kelley, C. F., Holz, D., Adeli Koudehi, M., Vogel, S. K., Burbaum, L., Mizuno, N., Vaylonis, D. and Schwille, P. (2021). Reconstitution of contractile actomyosin rings in vesicles. *Nat. Commun.* **12**, 2254. doi:10.1038/s41467-021-22422-7
- Liu, J., Fukuda, K., Xu, Z., Ma, Y.-Q., Hirbawi, J., Mao, X., Wu, C., Plow, E. F. and Qin, J. (2011). Structural basis of phosphoinositide binding to kindlin-2 protein pleckstrin homology domain in regulating integrin activation. *J. Biol. Chem.* **286**, 43334-43342. doi:10.1074/jbc.M111.295352
- Lu, F., Zhu, L., Bromberger, T., Yang, J., Yang, Q., Liu, J., Plow, E. F., Moser, M. and Qin, J. (2022). Mechanism of integrin activation by talin and its cooperation with kindlin. *Nat. Commun.* **13**, 2362. doi:10.1038/s41467-022-30117-w

- Ma, Y.-Q., Qin, J., Wu, C. and Plow, E. F. (2008). Kindlin-2 (Mig-2): a co-activator of $\beta 3$ integrins. *J. Cell Biol.* **181**, 439-446. doi:10.1083/jcb.200710196
- Martin, T. F. J. (2012). Role of PI(4,5)P2 in vesicle exocytosis and membrane fusion. In *Phosphoinositides II: The Diverse Biological Functions*, Vol. 59 (ed. T. Balla, M. Wymann and J. D. York), pp. 111-130. Springer Netherlands. doi:10.1007/978-94-007-3015-1_4
- Montanez, E., Ussar, S., Schifferer, M., Bösl, M., Zent, R., Moser, M. and Fässler, R. (2008). Kindlin-2 controls bidirectional signaling of integrins. *Genes Dev.* **22**, 1325-1330. doi:10.1101/gad.469408
- Moser, M., Nieswandt, B., Ussar, S., Pozgajova, M. and Fässler, R. (2008). Kindlin-3 is essential for integrin activation and platelet aggregation. *Nat. Med.* **14**, 325-330. doi:10.1038/nm1722
- Moser, M., Legate, K. R., Zent, R. and Fässler, R. (2009). The tail of integrins, talin, and kindlins. *Science* **324**, 895-899. doi:10.1126/science.1163865
- Orré, T., Joly, A., Karatas, Z., Kastberger, B., Cabriel, C., Böttcher, R. T., Lévêque-Fort, S., Sibarita, J.-B., Fässler, R., Wehrle-Haller, B. et al. (2021). Molecular motion and tridimensional nanoscale localization of kindlin control integrin activation in focal adhesions. *Nat. Commun.* **12**, 3104. doi:10.1038/s41467-021-23372-w
- Pollard, T. D. (1982). Myosin purification and characterization. *Methods Cell Biol.* **24**, 333-371. doi:10.1016/S0091-679X(08)60665-2
- Prévost, C., Tsai, F.-C., Bassereau, P. and Simunovic, M. (2017). Pulling membrane nanotubes from giant unilamellar vesicles. *J. Vis. Exp.* **130**, 56086. doi:10.3791/56086
- Rigaud, J.-L. and Lévy, D. (2003). Reconstitution of membrane proteins into liposomes. *Methods Enzymol.* **372**, 65-86. doi:10.1016/S0076-6879(03)72004-7
- Rossier, O., Oceau, V., Sibarita, J.-B., Leduc, C., Tessier, B., Nair, D., Gatterdam, V., Destaing, O., Albignès-Rizo, C., Tampé, R. et al. (2012). Integrins $\beta 1$ and $\beta 3$ exhibit distinct dynamic nanoscale organizations inside focal adhesions. *Nat. Cell Biol.* **14**, 1057-1067. doi:10.1038/ncb2588
- Saltel, F., Mortier, E., Hytönen, V. P., Jacquier, M.-C., Zimmermann, P., Vogel, V., Liu, W. and Wehrle-Haller, B. (2009). New PI(4,5)P2- and membrane proximal integrin-binding motifs in the talin head control $\beta 3$ -integrin clustering. *J. Cell Biol.* **187**, 715-731. doi:10.1083/jcb.200908134
- Schwartzman, M., Palma, M., Sable, J., Abramson, J., Hu, X., Sheetz, M. P. and Wind, S. J. (2011). Nanolithographic Control of the Spatial Organization of Cellular Adhesion Receptors at the Single-Molecule Level. *Nano Lett.* **11**, 1306-1312. doi:10.1021/nl104378f
- Sorre, B., Callan-Jones, A., Manzi, J., Goud, B., Prost, J., Bassereau, P. and Roux, A. (2012). Nature of curvature coupling of amphiphysin with membranes depends on its bound density. *Proc. Natl. Acad. Sci. USA* **109**, 173-178. doi:10.1073/pnas.1103594108
- Souissi, M., Pernier, J., Rossier, O., Giannone, G., Le Clairche, C., Helfer, E. and Sengupta, K. (2021). Integrin-functionalised giant unilamellar vesicles via gel-assisted formation: good practices and pitfalls. *Int. J. Mol. Sci.* **22**, 6335. doi:10.3390/ijms22126335
- Streicher, P., Nassoy, P., Bärmann, M., Dif, A., Marchi-Artzner, V., Brochard-Wyart, F., Spatz, J. and Bassereau, P. (2009). Integrin reconstituted in GUVs: a biomimetic system to study initial steps of cell spreading. *Biochim. Biophys. Acta. Biomembr.* **1788**, 2291-2300. doi:10.1016/j.bbmem.2009.07.025
- Sun, Z., Costell, M. and Fässler, R. (2019). Integrin activation by talin, kindlin and mechanical forces. *Nat. Cell Biol.* **21**, 25-31. doi:10.1038/s41556-018-0234-9
- Tadokoro, S., Shattil, S. J., Eto, K., Tai, V., Liddington, R. C., De Pereda, J. M., Ginsberg, M. H. and Calderwood, D. A. (2003). Talin binding to integrin β tails: a final common step in integrin activation. *Science* **302**, 103-106. doi:10.1126/science.1086652
- Takagi, J., Petre, B. M., Walz, T. and Springer, T. A. (2002). Global conformational rearrangements in integrin extracellular domains in outside-in and inside-out signaling. *Cell* **110**, 599-611. doi:10.1016/S0092-8674(02)00935-2
- Vigouroux, C., Henriot, V. and Le Clairche, C. (2020). Talin dissociates from RIAM and associates to vinculin sequentially in response to the actomyosin force. *Nat. Commun.* **11**, 3116. doi:10.1038/s41467-020-16922-1
- Wegener, K. L., Partridge, A. W., Han, J., Pickford, A. R., Liddington, R. C., Ginsberg, M. H. and Campbell, I. D. (2007). Structural basis of integrin activation by Talin. *Cell* **128**, 171-182. doi:10.1016/j.cell.2006.10.048
- Wehrle-Haller, B. (2012). Assembly and disassembly of cell matrix adhesions. *Curr. Opin. Cell Biol.* **24**, 569-581. doi:10.1016/j.cob.2012.06.010
- Weinberger, A., Tsai, F.-C., Koenderink, G. H., Schmidt, T. F., Itri, R., Meier, W., Schmatko, T., Schröder, A. and Marques, C. (2013). Gel-assisted formation of giant unilamellar vesicles. *Biophys. J.* **105**, 154-164. doi:10.1016/j.bpj.2013.05.024
- Wen, Y., Vogt, V. M. and Feigenson, G. W. (2018). Multivalent Cation-bridged PI(4,5)P2 clusters form at very low concentrations. *Biophys. J.* **114**, 2630-2639. doi:10.1016/j.bpj.2018.04.048
- Yang, J., Zhu, L., Zhang, H., Hirbawi, J., Fukuda, K., Dwivedi, P., Liu, J., Byzova, T., Plow, E. F., Wu, J. et al. (2014). Conformational activation of talin by RIAM triggers integrin-mediated cell adhesion. *Nat. Commun.* **5**, 5880. doi:10.1038/ncomms6880
- Ye, F., Petrich, B. G., Anekal, P., Lefort, C. T., Kasirer-Friede, A., Shattil, S. J., Ruppert, R., Moser, M., Fässler, R. and Ginsberg, M. H. (2013). The mechanism of kindlin-mediated activation of integrin $\alpha 11\beta 3$. *Curr. Biol.* **23**, 2288-2295. doi:10.1016/j.cub.2013.09.050
- Ye, F., Kim, S.-J. and Kim, C. (2014). Intermolecular transmembrane domain interactions activate integrin $\alpha 11\beta 3$. *J. Biol. Chem.* **289**, 18507-18513. doi:10.1074/jbc.M113.541888
- Yu, C., Law, J. B. K., Suryana, M., Low, H. Y. and Sheetz, M. P. (2011). Early integrin binding to Arg-Gly-Asp peptide activates actin polymerization and contractile movement that stimulates outward translocation. *Proc. Natl. Acad. Sci. USA* **108**, 20585-20590. doi:10.1073/pnas.1109485108

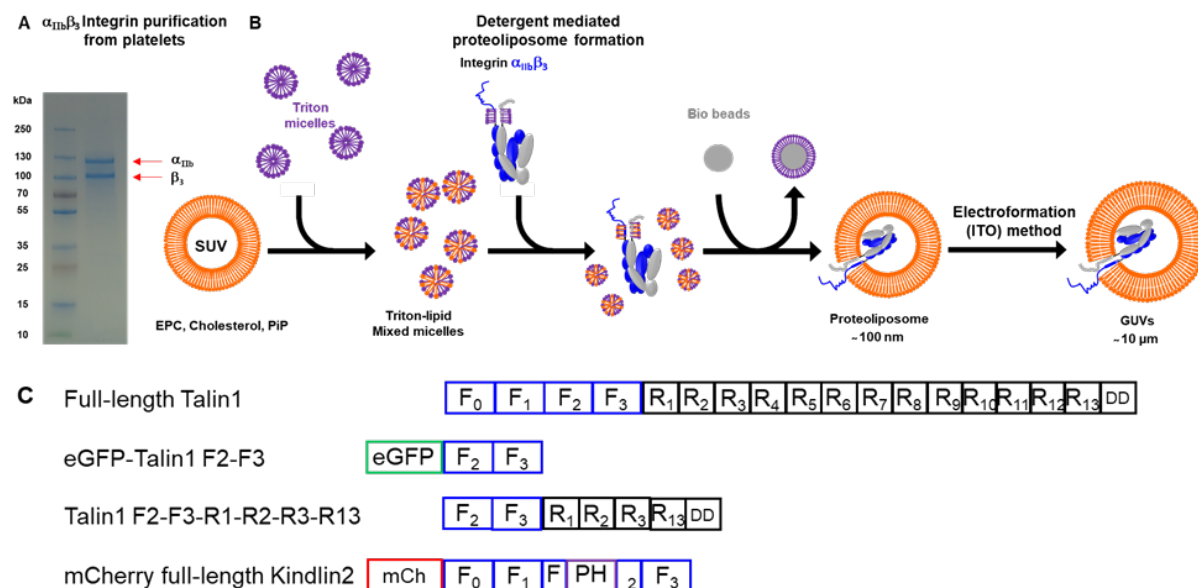


Fig. S1. Preparation of GUVs containing integrins.

(A) SDS-PAGE showing purified $\alpha_{IIb}\beta_3$ integrin from human platelets. (B) Detergent-mediated reconstitution used for the incorporation of purified integrin into proteoliposomes. GUV preparation with electroformation Indium tin oxide (ITO). (C) Schematic representation of domain organization of proteins used in this paper. F_0 to F_3 FERM subdomains (blue); R_1 to R_{13} rod domains (black); DD dimerization domain (black); PH domain (purple); enhanced green fluorescent protein (green) and mCherry (red).

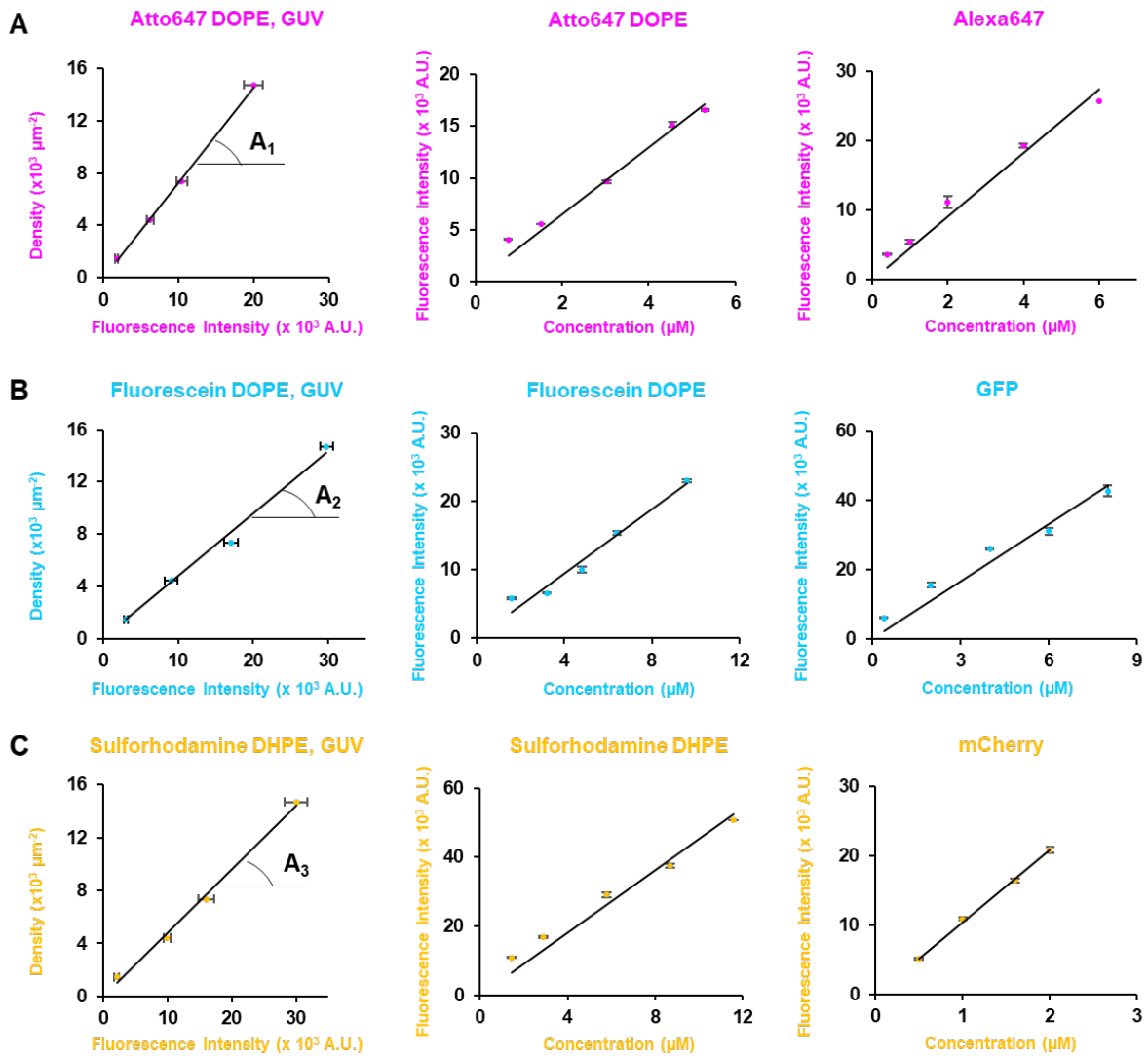


Fig. S2. Protein density calibration (used in Figure 3)

(A-C) The density of integrin, talin and kindlin in clusters (Fig. 3) is deduced from (left) the measurement of the fluorescence intensities of reference lipids respectively Atto647 DOPE (A), Fluorescein DOPE (B) and Sulforhodamine DHPE (C) at known density in GUVs, and the comparison of (right) the fluorescence of dyes used to label proteins in this study respectively Alexa 647, GFP and mCherry and (middle) respectively Atto647-DOPE, Fluorescein-DOPE and Sulforhodamine-DHPE in bulk at known concentrations (see Methods). The calibration constants A_1 , A_2 and A_3 are deduced from the slopes.

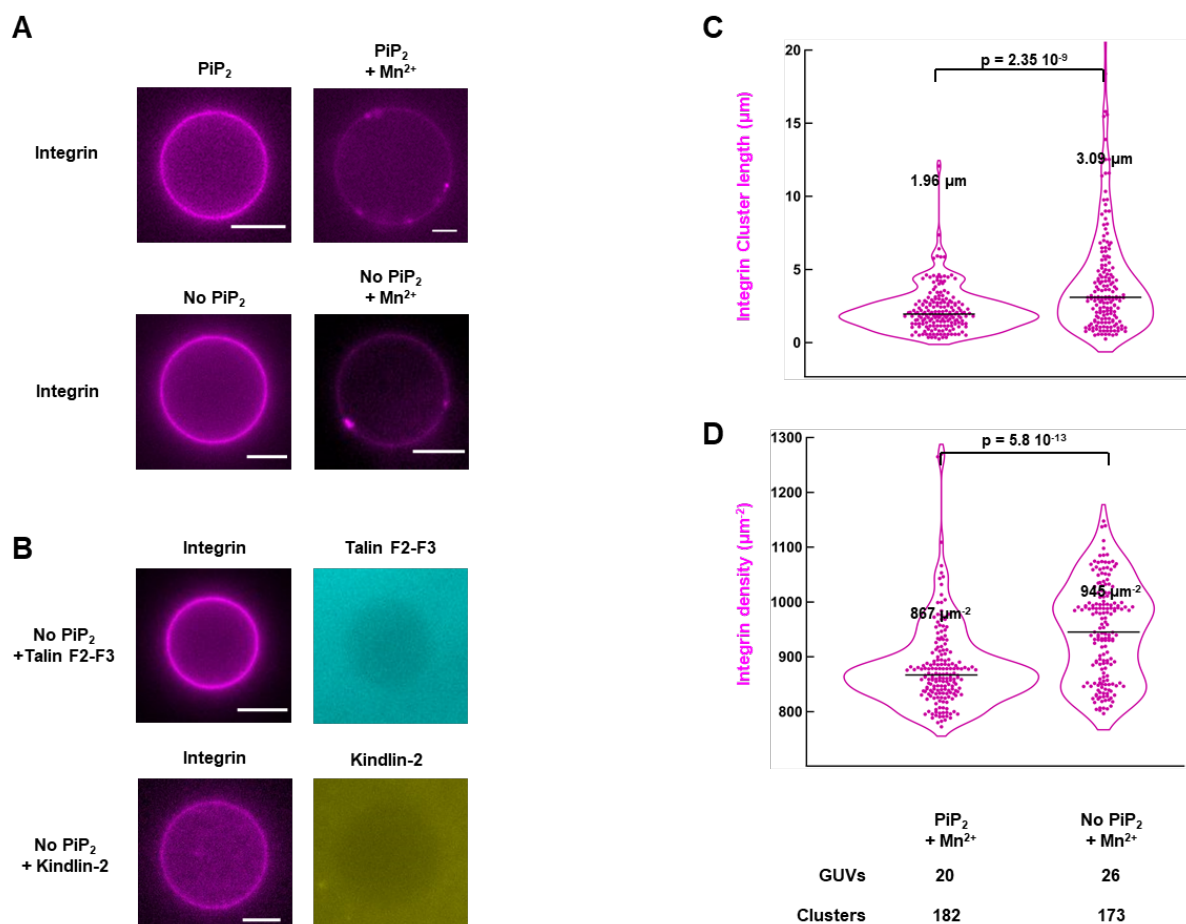


Fig. S3. MnCl₂ induces integrin clustering without PIP₂ whereas the recruitment of talin F2-F3 and kindlin-2 depends on PIP₂.

(A) Representative epifluorescence images of Alexa647-labeled integrin (magenta) reconstituted into GUVs with or without PIP₂, incubated without or with MnCl₂ (2 mM) alone. (B) Representative epifluorescence images of Alexa647-labeled integrin (magenta) reconstituted into GUVs without PIP₂, incubated without or with eGFP-talin F2-F3 (cyan, 200 nM) or mCherry-kindlin-2 (yellow, 200 nM). Violin representation of the length (C) and the density (D) of integrin, reconstituted into GUVs with or without PIP₂, in presence of MnCl₂ (2 mM). The number of analyzed GUVs, clusters and the medians are indicated. The results presented in this figure were confirmed in 2 to 4 independent experiments depending on the conditions. The p-values were obtained by a Mann-Whitney non parametric test at level 0.05. ns : not significant.

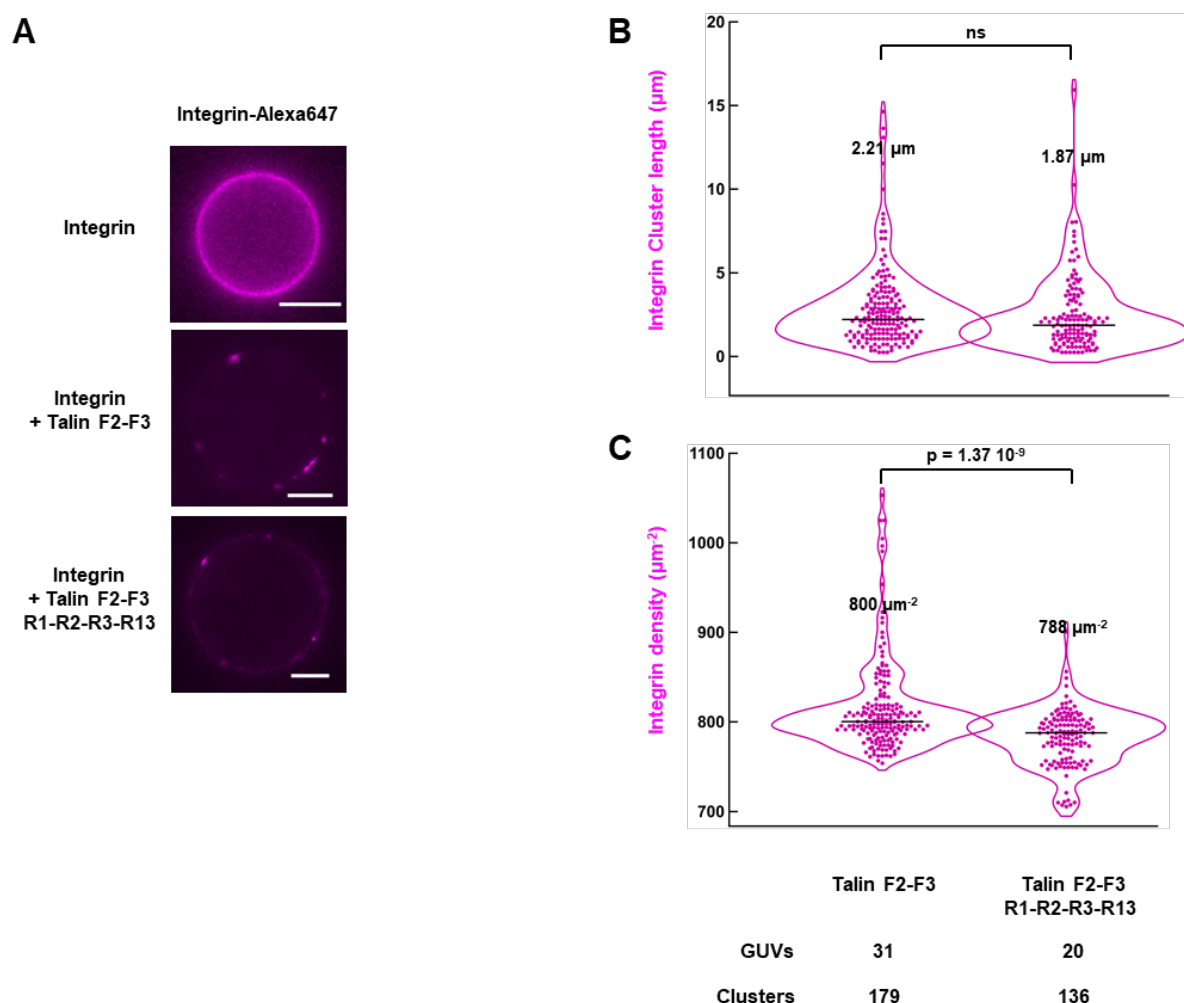


Fig. S4. Both monomeric talin F2-F3 and dimeric talin F2-F3-R1-R2-R3-R13 induce integrin clustering.

(A) Representative epifluorescence images of Alexa647-labeled integrin (magenta) reconstituted into GUVs incubated without or with eGFP-talin F2-F3 (200 nM) or talin F2-F3-R1-R2-R3-R13 (200 nM). Violin representation of the length (B) and the density (C) of integrin in presence of talin F2-F3 (200 nM) or talin F2-F3-R1-R2-R3-R13 (200 nM). The number of analyzed GUVs, clusters and the medians are indicated. The results presented in this figure were confirmed in 2 to 4 independent experiments depending on the conditions. The p-values were obtained by a Mann-Whitney non parametric test at level 0.05. ns : not significant.

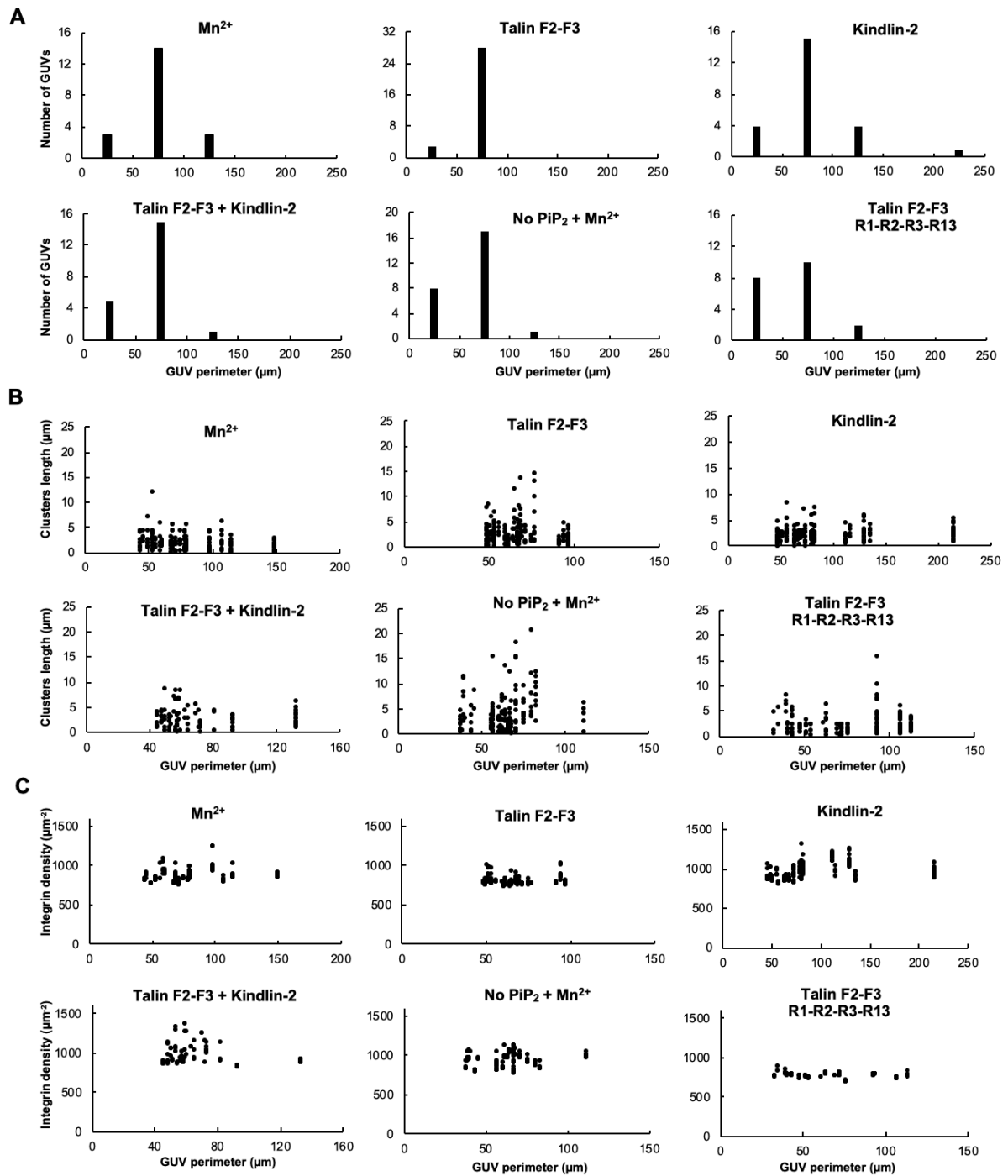


Fig. S5. Distribution and effect of GUV perimeter on integrin clustering (A) Distribution of the number of GUVs, **(B)** length of integrin clusters and **(C)** density of integrin clusters as a function of GUV perimeter for the different indicated conditions. The results presented in this figure were confirmed in 2 to 4 independent experiments depending on the conditions.

Table S1. Key resources

| Reagent type (species) or resource | Designation | Source or reference | Identifiers | Additional information |
|--|--|------------------------------------|---|--|
| Gene (Homo sapiens) | TLN1 | Human Genome Nomenclature Database | HGNC:11845 | |
| Gene (Homo sapiens) | FERMT2 | Human Genome Nomenclature Database | HGNC:15767 | |
| Strain, strain background (Escherichia coli) | BL21(DE3) | ThermoFisher Scientific | Cat# C600003 | Chemically competent cells |
| Recombinant DNA reagent | pGEX-6P1-GST-GFP-F2-F3 | This paper | | Human Talin1 F2-F3 |
| Recombinant DNA reagent | pETM-StrepTag II-F2-F3-R1-R2-R3-R13-6His | (Vigouroux et al., 2020) | | Human Talin1 F2-F3-R1-R2-R3-R13 |
| Recombinant DNA reagent | pGEX-6P1-GST-mCherry-Kindlin2-6His | This paper | | Human Kindlin2 |
| Chemical compound, drug | Alexa Fluor 647 succinimidyl ester | ThermoFisher Scientific | Cat# A37573 | For protein labeling |
| Chemical compound, drug | PLL-g-PEG | SuSoS | | Surface passivation |
| Chemical compound, drug | Triton X-100 | Sigma-Aldrich | Cat# X100 | protein reconstitution |
| Chemical compound, drug | Bio-beads | BIO-RAD | Cat# 152-3920 | protein reconstitution |
| Chemical compound, drug | Polyvinyl alcohol | Sigma-Aldrich | Cat# 8148941001 | GUVs preparation |
| Software, algorithm | FIJI | | https://imagej.net/Fiji/Downloads | |
| Software, algorithm | Icy | | https://icy.bioimageanalysis.org/download/ | |
| Other | EPC | Sigma-Aldrich | Cat# 840051 | L- α -phosphatidylcholine |
| Other | Cholesterol | Sigma-Aldrich | Cat# C8667 | |
| Other | Brain PI(4,5)P2 | Sigma-Aldrich | Cat# 840046 | L- α -phosphatidylinositol-4,5-bisphosphate |
| Other | PI(3,4,5)P3 | Sigma-Aldrich | Cat# 850156 | 1,2-dioleoyl-sn-glycero-3-phospho-(1'-myo-inositol-3',4',5'-trisphosphate) |